

# Observation of 300 K High Energy MagnetoDielectric Response in the Bilayer Manganite $(\text{La}_{0.4}\text{Pr}_{0.6})_{1.2}\text{Sr}_{1.8}\text{Mn}_2\text{O}_7$

Jinbo Cao,<sup>1</sup> Ram C. Rai,<sup>1</sup> Sonal Brown,<sup>1</sup> Janice L. Musfeldt,<sup>1</sup> Ronald Tackett,<sup>2</sup> Gavin Lawes,<sup>2</sup> Yongjie Wang,<sup>3</sup> Xing Wei,<sup>3</sup> Mircea Apostu,<sup>4</sup> Ramanathan Suryanarayanan,<sup>4</sup> and Alexandre Revcolevschi<sup>4</sup>

<sup>1</sup>Department of Chemistry, University of Tennessee, Knoxville, TN 37996 USA

<sup>2</sup>Department of Physics, Wayne State University, Detroit, MI 48201 USA

<sup>3</sup>National High Magnetic Field Laboratory, Florida State University, Tallahassee, FL 32310 USA

<sup>4</sup>Laboratoire de Physico-Chimie de l'Etat Solide, Univ. Paris-Sud., UMR 8182, 91405 Orsay, France

(Dated: March 23, 2022)

The discovery of magnetoelectric coupling and in particular of the magnetodielectric (MD) effect, e.g., field-induced change in dielectric constant  $\epsilon_1$ , has attracted attention due to both potential utilization in multifunctional devices and the desire to understand the fundamental physics underlying multiferroic materials.<sup>1,2,3,4,5,6,7,8</sup> For instance, rare earth manganites such as  $\text{TbMnO}_3$ ,  $\text{HoMnO}_3$ ,  $\text{YMnO}_3$ , and  $\text{DyMn}_2\text{O}_5$  display sizable static MD effects at low temperature, demonstrating that dielectric contrast can be achieved by physical tuning through various magnetic transitions in  $H-T$  space.<sup>2,3,4</sup> Cubic spinels such as  $\text{CdCr}_2\text{S}_4$  and  $\text{HgCr}_2\text{S}_4$  present even larger static MD contrast, attributed to relaxational dynamics driven by magnetization in the field.<sup>5,6,7</sup> More recently, 300 K MD behavior was reported in mixed valent  $\text{LuFe}_2\text{O}_4$  and attributed to charge ordering effects.<sup>8</sup> Mn-doped  $\text{BiFeO}_3$  also exhibits a potentially tunable room temperature MD effect due to enhanced thermal fluctuations near the Néel temperature.<sup>9</sup> Discovery of large MD effects in other materials combined with mechanistic understanding of magnetoelectric cross-coupling is of fundamental interest and may hold promise for next-generation memory devices.

Static dielectric properties are typically measured in a parallel plate/capacitance geometry at low frequencies (Hz - MHz).<sup>5,7,8</sup> Challenges with this technique include contact problems, potential dead layers, and edge effects.<sup>10,11</sup> A contactless technique, such as optical spectroscopy, eliminates these issues. At the same time, the electromagnetic spectrum is very broad. This opens the possibility of exploiting changes in  $\epsilon_1$  over a wide energy range, essentially as a multi- (rather than single-) channel information storage system. The high energy magnetodielectric (HEMD) effect was recently discovered in several materials including inhomogeneously mixed-valent  $\text{K}_2\text{V}_3\text{O}_8$  ( $\sim 5\%$  at 30 T near 1.2 eV), Kagomé staircase compound  $\text{Ni}_3\text{V}_2\text{O}_8$  ( $\sim 16\%$  at 30 T near 1.3 eV), and hexagonal multiferroic  $\text{HoMnO}_3$  ( $\sim 8\%$  at 20 T near 1.8 eV).<sup>12,13,14</sup> In these materials, the HEMD effect derives from spin-lattice-charge mixing effects. Part of our continuing strategy to increase dielectric contrast centers on the exploitation of electronic mechanisms such as metal-insulator transitions, charge ordering, and orbital ordering that are known to drive changes in the optical constants.<sup>15,16</sup> Metal-insulator transitions are common with decreasing temperature, but they are rarely

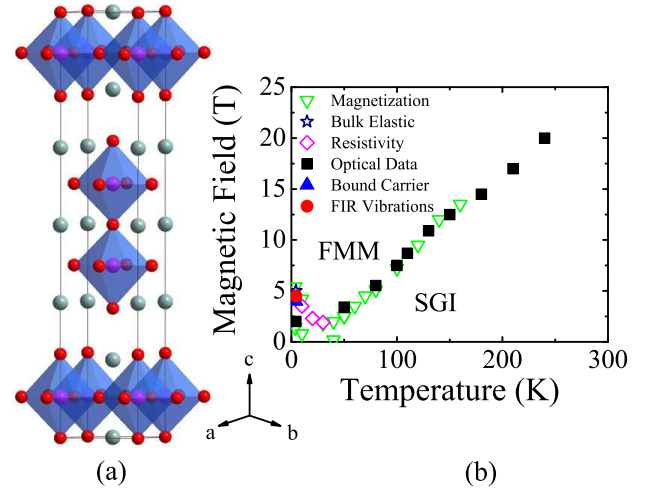


FIG. 1: (Color online) (a) 300 K crystal structure of  $(\text{La}_{0.4}\text{Pr}_{0.6})_{1.2}\text{Sr}_{1.8}\text{Mn}_2\text{O}_7$ , with O (red/black), Mn-containing octahedra (magenta/gray), and rare/alkaline earth ions (olive/light gray).<sup>17</sup> (b)  $H-T$  phase diagram, extracted from optical properties data (■) for  $H \parallel c$ . Data are taken with increasing field. Selected magnetization, magnetostriction, and resistivity results are shown for comparison.<sup>19,20,21,22</sup> The spin-glass insulator to ferromagnetic metal transition is robust at low temperature but diffuse at high temperatures.

induced by magnetic field. Here, we report a colossal HEMD response in  $(\text{La}_{0.4}\text{Pr}_{0.6})_{1.2}\text{Sr}_{1.8}\text{Mn}_2\text{O}_7$ , behavior that results from a magnetic field driven spin-glass insulator to ferromagnetic metal transition. Remnants of the transition also drive the HEMD effect at room temperature.

$(\text{La}_{0.4}\text{Pr}_{0.6})_{1.2}\text{Sr}_{1.8}\text{Mn}_2\text{O}_7$  derives from the  $\text{La}_{1.2}\text{Sr}_{1.8}\text{Mn}_2\text{O}_7$  parent compound, a double-layer perovskite crystallizing in a body-centered tetragonal structure (space group  $I4/mmm$ ), as shown in Fig. 1 (a).<sup>17</sup> The  $(\text{La}_{1-z}\text{Pr}_z)_{1.2}\text{Sr}_{1.8}\text{Mn}_2\text{O}_7$  series provides an opportunity to investigate the physical properties of bilayer manganites as a function of chemical composition, tuning that gives rise to a rich phase diagram in this and related systems.<sup>18,19</sup> The parent compound ( $z=0$ ) displays a paramagnetic insulator to ferromagnetic metal transition at  $T_c=120$  K. With increasing Pr substitution,

$T_c$  decreases, and eventually disappears ( $z=0.6$ ), establishing a new spin glass insulating ground state.<sup>18,19</sup> The ferromagnetic metallic state that is suppressed by chemical pressure in  $(\text{La}_{0.4}\text{Pr}_{0.6})_{1.2}\text{Sr}_{1.8}\text{Mn}_2\text{O}_7$  is recovered under magnetic field, as revealed in the  $H-T$  phase diagram (Fig. 1 (b)). Transport, magnetization, elastic, and optical measurements demonstrate that the critical field is  $\sim 5$  T at 4.2 K, above which the system is in the ferromagnetic metallic state.<sup>19,20,21,22</sup> The local structure changes dramatically with applied magnetic field.<sup>23</sup> Both Mn-O stretching and bending modes soften through the field-driven transition.<sup>19</sup>

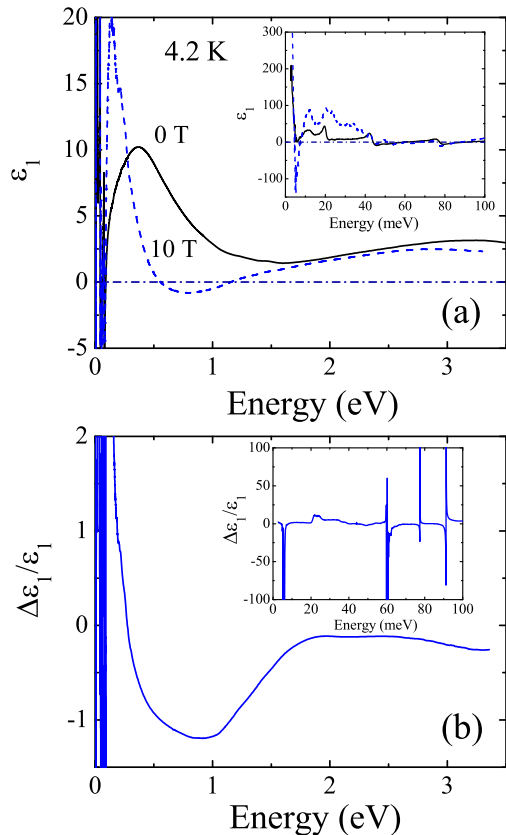


FIG. 2: (Color online) (a) Dielectric response of  $(\text{La}_{0.4}\text{Pr}_{0.6})_{1.2}\text{Sr}_{1.8}\text{Mn}_2\text{O}_7$  for  $H=0$  (solid line) and 10 T (dashed line) ( $H \parallel c$ ) at 4.2 K, as determined by Kramers-Kronig analysis of the measured reflectance. (b) The high-energy dielectric contrast,  $\Delta\epsilon_1/\epsilon_1$ , for  $H=0$  and 10 T.

Figure 2 (a) displays the real part of the dielectric response as a function of energy at low temperature. At zero field, the dispersive response exhibits typical behavior of a semiconductor, with an overall positive  $\epsilon_1$  except for the regions with strong phonon dispersions. The dispersive response of the Pr-substituted compound in the high field state is different due to the change in the ground state.  $\epsilon_1$  crosses zero at the screened plasma energy  $\sim 1.2$  eV, recrosses into posi-

tive territory at  $\sim 0.6$  eV, and crosses zero several times again at low energy due to the dispersive phonon behavior (inset, Fig. 2 (a)). To emphasize the difference between the zero and high field dielectric response of  $(\text{La}_{0.4}\text{Pr}_{0.6})_{1.2}\text{Sr}_{1.8}\text{Mn}_2\text{O}_7$ , we plot the dielectric contrast  $\Delta\epsilon_1/\epsilon_1 = [\epsilon_1(E, H) - \epsilon_1(E, 0)]/\epsilon_1(E, 0)$  (Fig. 2 (b)). The size of the dielectric contrast depends on energy. It is as large as  $\sim 100\%$  near 0.8 eV. This is the range of Mn charge transfer and on-site excitations. In selected phonon regimes (near 6, 60, 77, 90 meV), the dielectric contrast is enormous, on the order of 10000%. The 4.2 K dielectric contrast is a direct consequence of the robust low temperature spin-glass insulator to ferromagnetic metal transition and strong spin-lattice-charge cross coupling in  $(\text{La}_{0.4}\text{Pr}_{0.6})_{1.2}\text{Sr}_{1.8}\text{Mn}_2\text{O}_7$ .

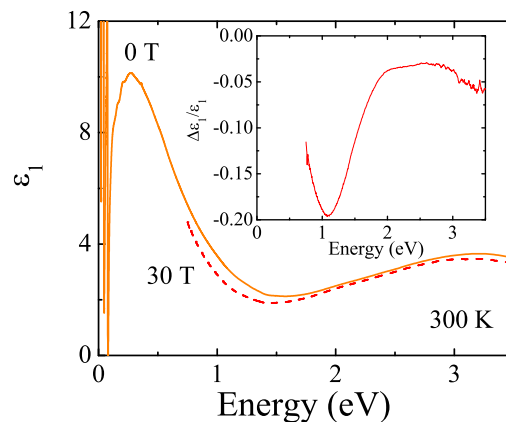


FIG. 3: (Color online) Dielectric response of  $(\text{La}_{0.4}\text{Pr}_{0.6})_{1.2}\text{Sr}_{1.8}\text{Mn}_2\text{O}_7$  for  $H=0$  (solid line) and 30 T (dashed line) ( $H \parallel c$ ) at 300 K, as determined by Kramers-Kronig analysis of the measured reflectance. The inset displays the high-energy dielectric contrast,  $\Delta\epsilon_1/\epsilon_1$ , for  $H=0$  and 30 T.

It is clearly desirable to design and assemble multifunctional devices that operate at higher temperatures. Materials that exhibit room temperature magnetoelectric coupling are therefore needed. To this end, we have employed the remnants of the spin-glass insulator to ferromagnetic metal transition in  $(\text{La}_{0.4}\text{Pr}_{0.6})_{1.2}\text{Sr}_{1.8}\text{Mn}_2\text{O}_7$  to achieve a 300 K HEMD effect. Figure 3 displays the room temperature dielectric properties of  $(\text{La}_{0.4}\text{Pr}_{0.6})_{1.2}\text{Sr}_{1.8}\text{Mn}_2\text{O}_7$  at 0 and 30 T. The dispersive response shifts to lower energy in applied magnetic field, consistent with the previous observation of redshifted oscillator strength in the ferromagnetic metallic state.<sup>19</sup> Strikingly, the dielectric contrast displays a 20% change near 1.1 eV (inset of Fig. 3).<sup>24</sup> Although weaker than that at 4.2 K, this finding demonstrates that electronic transitions can be harnessed for 300 K HEMD effects.

The HEMD effect in  $(\text{La}_{0.4}\text{Pr}_{0.6})_{1.2}\text{Sr}_{1.8}\text{Mn}_2\text{O}_7$  is substantially larger than that in mixed-valent  $\text{K}_2\text{V}_3\text{O}_8$ , Kagomé staircase compound  $\text{Ni}_3\text{V}_2\text{O}_8$ , and frustrated

HoMnO<sub>3</sub>, oxides where magnetoelastic/magnetolectric coupling is important.<sup>12,13,14</sup> As mentioned previously, this stronger dielectric contrast is directly related to exploiting the field-induced insulator to metal transition. Reviewing the Tomioka-Tokura global phase diagram in complex perovskites,<sup>18</sup> the title compound is sitting in close proximity to the phase boundary and is therefore susceptible to physical tuning - even when the transition itself is no longer well-defined. Control of disorder therefore provides an important route for tuning the HEMD effect.<sup>18,19</sup>

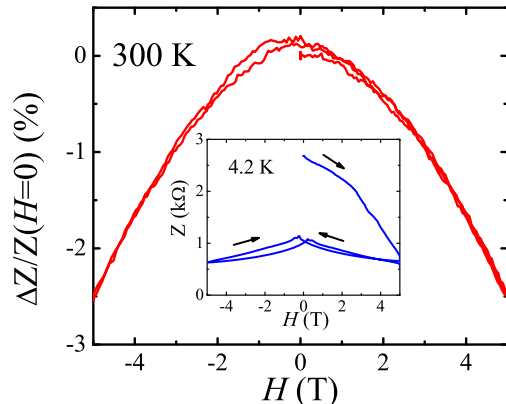


FIG. 4: (Color online) The magneto-impedance contrast of  $(\text{La}_{0.4}\text{Pr}_{0.6})_{1.2}\text{Sr}_{1.8}\text{Mn}_2\text{O}_7$  as a function of magnetic field ( $H \parallel c$ ) at 300 K. The inset displays the magnitude of the impedance as a function of magnetic field ( $H \parallel c$ ) at 4.2 K. The sample was zero-field cooled.

It is interesting to compare the HEMD effect in  $(\text{La}_{0.4}\text{Pr}_{0.6})_{1.2}\text{Sr}_{1.8}\text{Mn}_2\text{O}_7$  with static results. Due to the large DC conductivity of these single crystal samples, we investigate the low frequency magnetic response in terms of the impedance rather than  $\epsilon_1$ .<sup>25,26</sup> The inset of Fig. 4 displays the low frequency (30 kHz) impedance as a function of magnetic field at 4.2 K. The high impedance insulating state at 0 T is suppressed with increasing magnetic field, leading to a large change in impedance between 0 and 5 T. As the field decreases towards 0 T, there is a small increase in impedance, but the sample remains trapped in the metastable low impedance state. The phase of the complex impedance displays similar behavior. Field-induced transitions and trapping in a metastable state have been observed in resistivity measurements of  $(\text{La}_{0.4}\text{Pr}_{0.6})_{1.2}\text{Sr}_{1.8}\text{Mn}_2\text{O}_7$ ,<sup>27</sup> and were attributed to the strong magnetoresistive coupling in this system. This static spin-charge coupling persists to higher temperatures. The main panel of Fig. 4 displays the 300 K magneto-impedance contrast as a function of magnetic field. The impedance of the sample changes up

to 2.5% in a 5 T applied field. This magneto-impedance is completely non-hysteretic, different from that at low temperatures. Similar magneto-impedance has been observed close to the ferromagnetic ordering temperature in other manganites,<sup>25,26</sup> and was attributed to the dependence of the skin depth on both magnetic field and frequency. Clearly, these room temperature effects represent significant spin-charge coupling persisting to temperatures well above the magnetic transition temperature, in line with the 300 K HEMD effect.

To summarize, we observed a large HEMD effect in the bilayer manganite  $(\text{La}_{0.4}\text{Pr}_{0.6})_{1.2}\text{Sr}_{1.8}\text{Mn}_2\text{O}_7$ , a direct consequence of field driven spin-glass insulator to ferromagnetic metal transition. The remnants of the transition can be used to achieve dielectric contrast at room temperature. This discovery suggests that electronic mechanisms such as the metal-insulator transition, charge ordering, and orbital ordering can be exploited to give substantial dielectric contrast in other materials.

## Experimental

Single crystals of  $(\text{La}_{0.4}\text{Pr}_{0.6})_{1.2}\text{Sr}_{1.8}\text{Mn}_2\text{O}_7$  were grown from sintered rods of same nominal composition by the floating-zone technique, using a mirror furnace.<sup>17</sup> Typical crystal dimensions were  $\approx 4 \times 5 \times 2$  mm<sup>3</sup>. They were cleaved to yield a shiny surface corresponding to the  $ab$  plane.

Near normal  $ab$  plane reflectance of  $(\text{La}_{0.4}\text{Pr}_{0.6})_{1.2}\text{Sr}_{1.8}\text{Mn}_2\text{O}_7$  was measured over a wide energy range (3.7 meV - 6.5 eV) using a series of different spectrometers as described previously.<sup>19</sup> A Kramers-Kronig analysis was employed to obtain the optical constants,<sup>28</sup> particularly the dispersive part of the dielectric response as  $\tilde{\epsilon}(E) = \epsilon_1(E) + i\epsilon_2(E)$ . The magneto-optical properties were measured at the National High Magnetic Field Laboratory in Tallahassee, FL, using two different spectrometers and both superconducting and resistive magnets.<sup>19</sup> Experiments were performed at 4.2 and 300 K for  $H \parallel c$ .<sup>19</sup> The field-induced changes in the measured reflectance were studied by taking the ratio of reflectance at each field and reflectance at zero field, i.e.,  $[R(H)/R(H=0 \text{ T})]$ . To obtain the high field dielectric properties, we renormalized the zero-field absolute reflectance with the high-field reflectance ratios, and recalculated  $\epsilon_1(E)$  using Kramers-Kronig techniques.<sup>28</sup>

Impedance measurements were carried out at 30 kHz, using an Agilent 4284A LCR meter in a two-wire configuration with the AC current parallel to the applied magnetic field. The high temperature impedance was corrected for the contribution from the probe, which is negligible at 4.2 K.

## Acknowledgements

Work at the University of Tennessee is supported by the Materials Science Division, Basic Energy Sciences, U.S. Department of Energy (DE-FG02-01ER45885). The international aspects of this research were supported by the National Science Foundation (INT-019650) at UT and the Jane and Frank Warchol Foundation at Wayne State. A portion of this work was performed at the NHMFL, which is supported by NSF Cooperation Agreement DMR-0084173 and by the State of Florida.

- 
- <sup>1</sup> N. S. Rogado, J. Li, A. W. Sleight, and M. A. Subramanian, *Adv. Mater.* **17**, 2225 (2005).
  - <sup>2</sup> T. Kimura, T. Goto, H. Shintani, K. Ishizaka, T. Arima, and Y. Tokura, *Nature* **426**, 55 (2003).
  - <sup>3</sup> B. Lorenz, Y. Q. Wang, Y. Y. Sun, and C. W. Chu, *Phys. Rev. B* **70**, 212412 (2004).
  - <sup>4</sup> N. Hur, S. Park, P. A. Sharma, S. Guha, and S-W. Cheong, *Phys. Rev. Lett.* **93**, 107207 (2004).
  - <sup>5</sup> J. Hemberger, P. Lunkenheimer, R. Fichtl, H.-A. Krug von Nidda, V. Tsurkan, and A. Loidl, *Nature (London)* **434**, 364 (2005).
  - <sup>6</sup> P. Lunkenheimer, R. Fichtl, J. Hemberger, V. Tsurkan, and A. Loidl, *Phys. Rev. B* **72**, 060103(R) (2005).
  - <sup>7</sup> S. Weber, P. Lunkenheimer, R. Fichtl, J. Hemberger, V. Tsurkan, and A. Loidl, *Phys. Rev. Lett.* **96**, 157202 (2006).
  - <sup>8</sup> M. A. Subramanian, T. He, J. Chen, N. S. Rogado, T. G. Calvarese, and A. W. Sleight, *Adv. Mater.* **18**, 1737 (2006).
  - <sup>9</sup> C.-H. Yang, T.Y. Koo, and Y.H. Jeong, *Solid State Commun.* **134**, 299 (2005).
  - <sup>10</sup> C. Zhou and D. M. Newns, *J. Appl. Phys.* **82**, 3081 (1997).
  - <sup>11</sup> M. Stengel and N. A. Spaldin, *Nature* **443**, 679 (2006).
  - <sup>12</sup> R. C. Rai, J. Cao, J. L. Musfeldt, D. J. Singh, X. Wei, R. Jin, Z. X. Zhou, B. C. Sales, and D. Mandrus, *Phys. Rev. B* **73**, 075112 (2006).
  - <sup>13</sup> R. C. Rai, J. Cao, S. Brown, J. L. Musfeldt, D. Kasinathan, D. J. Singh, G. Lawes, N. Rogado, R. J. Cava, and X. Wei (unpublished).
  - <sup>14</sup> R. C. Rai, J. Cao, J. L. Musfeldt, S.B. Kim, S.-W. Cheong, and X. Wei (unpublished).
  - <sup>15</sup> W. J. Padilla, D. Mandrus, and D. N. Basov, *Phys. Rev. B* **66**, 035120 (2002).
  - <sup>16</sup> R. Rückamp, E. Benckiser, M. W. Haverkort, H. Roth, T. Lorenz, A. Freimuth, L. Jongen, A. Möller, G. Meyer, P. Reutler, B. Büchner, A. Revcolevschi, S-W. Cheong, C. Sekar, G. Krabbes, and M. Grüninger, *New J. Phys.* **7**, 144 (2005).
  - <sup>17</sup> M. Apostu, R. Suryanarayanan, A. Revcolevschi, H. Ogasawara, M. Matsukawa, M. Yoshizawa, and N. Kobayashi, *Phys. Rev. B* **64**, 012407 (2001).
  - <sup>18</sup> Y. Tomioka and Y. Tokura, *Phys. Rev. B* **70**, 014432 (2004).
  - <sup>19</sup> J. Cao, J. T. Haraldsen, R. C. Rai, S. Brown, J. L. Musfeldt, Y. J. Wang, X. Wei, M. Apostu, R. Suryanarayanan, and A. Revcolevschi, *Phys. Rev. B* **74**, 045113 (2006).
  - <sup>20</sup> I. Gordon, P. Wagner, V. V. Moshchalkov, Y. Bruynseraede, M. Apostu, R. Suryanarayanan, and A. Revcolevschi, *Phys. Rev. B* **64**, 092408 (2001).
  - <sup>21</sup> M. Matsukawa, M. Chiba, A. Akasaka, R. Suryanarayanan, M. Apostu, A. Revcolevschi, S. Nimori, and N. Kobayashi, *Phys. Rev. B* **70**, 132402 (2004).
  - <sup>22</sup> Y. Nakanishi, K. Shimomura, T. Kumagai, M. Matsukawa, M. Yoshizawa, M. Apostu, R. Suryanarayanan, A. Revcolevschi, and S. Nakamura, (unpublished).
  - <sup>23</sup> A. Gukasov, F. Wang, B. Anighoefer, L. He, R. Suryanarayanan, and A. Revcolevschi, *Phys. Rev. B* **72**, 092402 (2005).
  - <sup>24</sup> The HEMD effect in the far and middle infrared region could not be assessed in our experiments at the NHMFL. We anticipate that the dielectric contrast will be larger based upon its low temperature behavior.
  - <sup>25</sup> H. Qin, J. Hu, J. Chen, Y. Wang, and Z. Wang, *J. Appl. Phys.* **91**, 10003 (2002).
  - <sup>26</sup> G. M. B. Castro, A. R. Rodrigues, F. L. A. Machado, A. E. P. de Araujo, R. F. Jardim, and A. K. Nigam, *J. Alloys and Compounds* **369**, 108 (2004).
  - <sup>27</sup> M. Matsukawa, K. Akasaka, H. Noto, R. Suryanarayanan, S. Nimori, M. Apostu, A. Revcolevschi, and N. Kobayashi, *Phys. Rev. B* **72**, 064412 (2005).
  - <sup>28</sup> F. Wooten, *Optical Properties of Solids* (Academic Press, New York, 1972).